Cellular/Molecular

Nanodomains of Single Ca^{2+} Channels Contribute to Action Potential Repolarization in Cortical Neurons

Andreas Müller,[1] Maria Kukley,[1] Mischa Uebachs,[2] Heinz Beck,[2] and Dirk Dietrich[1]
Departments of [1]Neurosurgery and [2]Epileptology, University Clinic Bonn, 53105 Bonn, Germany

The precise shape of action potentials in cortical neurons is a key determinant of action potential-dependent Ca^{2+} influx, as well as of neuronal signaling, on a millisecond scale. In cortical neurons, Ca^{2+}-sensitive K^+ channels, or BK channels (BKChs), are crucial for action potential termination, but the precise functional interplay between Ca^{2+} channels and BKChs has remained unclear. In this study, we investigate the mechanisms allowing for rapid and reliable activation of BKChs by single action potentials in hippocampal granule cells and the impact of endogenous Ca^{2+} buffers. We find that BKChs are operated by nanodomains of single Ca^{2+} channels. Using a novel approach based on a linear approximation of buffered Ca^{2+} diffusion in microdomains, we quantitatively analyze the prolongation of action potentials by the Ca^{2+} chelator BAPTA. This analysis allowed us to estimate that the mean diffusional distance for Ca^{2+} ions from a Ca^{2+} channel to a BKCh is ~13 nm. This surprisingly short diffusional distance cannot be explained by a random distribution of Ca^{2+} channels and renders the activation of BKChs insensitive to the relatively high concentrations of endogenous Ca^{2+} buffers in hippocampal neurons. These data suggest that tight colocalization of the two types of channels permits hippocampal neurons to regulate global Ca^{2+} signals by a high cytoplasmic Ca^{2+} buffer capacity without affecting the fast and brief activation of BKChs required for proper repolarization of action potentials.

Key words: **microdomains; calbindin; calcium buffer; action potential; BK channel/Slo; calcium; diffusion; hippocampus; patch clamp**

Introduction

Ca^{2+} is a versatile intracellular messenger that translates neuronal activity into a variety of short- and long-term cellular actions such as transmitter release, gene transcription, or neuronal cell death. Action potentials represent one of the most potent Ca^{2+} influx pathways because they depolarize large parts of the neuronal membrane and thereby open many voltage-gated Ca^{2+} channels. The amount of Ca^{2+} entering per action potential is crucially determined by the shape of the action potential, because most influx occurs during the repolarization of the action potential (Llinas et al., 1982). For this reason, the precise regulation of the duration of action potentials is important to many neuronal functions, and neurons must possess effective mechanisms to limit Ca^{2+} influx during action potentials and to avoid an overload with Ca^{2+} during repetitive spiking activity. Many cortical neurons use large-conductance Ca^{2+}-activated potassium channels (BKChs) for that purpose. These channels have the unique property that they are activated by both the depolarizing voltage as well as by the rise in the intracellular free Ca^{2+} concentration during an action potential, which therefore provide ideal means for a negative feedback mechanism limiting the amount of Ca^{2+} entry (Vergara et al., 1998; Sah and Faber, 2002; Lu et al., 2006).

Although the biophysical properties of BKChs make them ideally suited to keep action potentials narrow and limit Ca^{2+} entry, it is unclear how neurons manage to use them effectively. For example, single action potentials potently activate BKChs but primarily avoid recruitment of other Ca^{2+}-activated channels, such as Ca^{2+}-activated, nonselective cation channels, which would depolarize the membrane and counteract the effect of BKChs (Partridge et al., 1994). Furthermore, BKChs remain open only for a brief period of time (a few milliseconds) (Shao et al., 1999) and therefore do not interfere with repetitive spiking, which is necessary for high-frequency encoding of neuronal information. It is therefore a fundamental question as to how neurons are able to assure the selective, rapid, brief, and reliable activation of BKChs during action potentials.

Neurons typically contain some kind of Ca^{2+}-binding proteins that allow them a more complex signal integration by shaping the spatiotemporal spread of Ca^{2+} signals (Maeda et al., 1999; Jackson and Redman, 2003). Ca^{2+} buffers can potentially impose severe limitations on the speed, reliability, and duration of the activation of BKChs. Indeed, it is known that the Ca^{2+}-binding protein calbindin-D_{28k} strongly limits the activation of BKChs in certain sensory neurons (Roberts, 1994). Several cortical neurons, such as hippocampal granule cells, also contain large amounts of calbindin-D_{28k} (Muller et al., 2005). However, it is as yet unknown whether endogenous Ca^{2+} buffers have any impact on the action potential-induced activation of BKChs in cortical neurons.

Received Sept. 1, 2006; revised Nov. 27, 2006; accepted Nov. 27, 2006.

This work was supported by the Deutsche Forschungsgemeinschaft (SFB TR3 C5, GK 246), University Clinic Bonn grants (BONFOR), and the Gertrud-Reemtsma-Stiftung of the Max-Planck-Gesellschaft. We thank Roland Krüppel for advice on the Monte Carlo simulation and for critically reading this manuscript. We are grateful to Pia Stausberg for excellent technical assistance.

Correspondence should be addressed to Dr. Dirk Dietrich, Department of Neurosurgery, NCH U1 R035, Experimental Neurophysiology, University Clinic Bonn, Sigmund-Freud Street 25 , D-53105 Bonn, Germany. E-mail: dirk.dietrich@ukb.uni-bonn.de.

DOI:10.1523/JNEUROSCI.3816-06.2007

 0270-6474/07/270483-13$15.00/0

In this study, we investigate the impact of endogenous and exogenous Ca^{2+} buffers on the repolarizing efficacy of BKChs and report that cortical neurons use a precise strategic placement of BKChs to optimize their recruitment by single action potentials under most physiological circumstances.

Materials and Methods

Preparation of slices and recording configuration in current clamp and hybrid clamp. Wistar rats (20–40 d old) or adult mice (mice were used for experiments shown in Fig. 2, *E* and *F*, calbindin−/− mice) were decapitated under ether anesthesia. The brains were rapidly dissected and chilled in 4°C cutting solution consisting of the following (in mM): 87 NaCl, 2.5 KCl, 1.25 NaH_2PO_4, 7 $MgSO_4$, 0.5 $CaCl_2$, 25 $NaHCO_3$, 25 glucose, 75 sucrose, gassed with a 95% O_2/5% CO_2 mixture, pH 7.4. Horizontal hippocampal slices (400 μm) were prepared with a Vibratome (Leica, Nussloch, Germany). Until recording, slices were stored at room temperature in artificial CSF (ACSF) containing the following (in mM): 124 NaCl, 3 KCl, 1.25 NaH_2PO_4, 2 $MgSO_4$, 2 $CaCl_2$, 26 $NaHCO_3$, 10 glucose, 300 mOsm osmolarity, pH 7.4, gassed with a 95% O_2/5% CO_2 mixture. For recording, slices were transferred to an interface chamber perfused with ACSF (35 ± 0.5°C) that contained the following (in mM): 125 NaCl, 3 KCl, 2 $CaCl_2$, 2 $MgCl_2$, 1.25 NaH_2PO_4, 20.3 $NaHCO_3$, 12 D-glucose, pH 7.4, gassed with 95% O_2/5% CO_2. Patch pipettes had resistances between 4 and 5 MΩ. The standard pipette solution was free of any Ca^{2+} chelators and contained the following (in mM): 140 K^+-gluconate, 0.5 $MgCl_2$, 4 NaCl, 10 HEPES, 5 KCl. A small amount of EGTA (20 μM) was added to the solution to balance Ca^{2+} contamination of salts. When Ca^{2+} chelators [1,2-bis(2-aminophenoxy)ethane-*N*,*N*,*N*′,*N*′-tetraacetic acid (BAPTA) or EGTA] were present, we supplemented $CaCl_2$ to maintain a free [Ca^{2+}] of ~38 nM (calculated with "webmaxc" available at http://www.stanford.edu/~cpatton/maxc.html) (Patton et al., 2004). Four different pipette solutions were used (3, 6, and 10 mM BAPTA; 10 mM EGTA). Solution 1 contained the following (in mM): 120 K^+-gluconate, 4 NaCl, 0.52 $MgCl_2$, 3 K_4-BAPTA, 0.02 EGTA, 10 HEPES, 0.25 $CaCl_2$, 5 KCl. Solution 2 contained the following (in mM): 115 K^+-gluconate, 4 NaCl, 0.54 $MgCl_2$, 6 K_4-BAPTA, 0.02 EGTA, 10 HEPES, 0.49 $CaCl_2$, 5 KCl. Solution 3 contained the following (in mM): 80 K^+-gluconate, 4 NaCl, 0.57 $MgCl_2$, 10 K_4-BAPTA, 0.02 EGTA, 10 HEPES, 0.81 $CaCl_2$, 5 KCl. Solution 4 contained the following (in mM): 10 EGTA, 140 K^+-gluconate, 4 NaCl, 0.84 $MgCl_2$, 10 HEPES, 2.56 $CaCl_2$, 5 KCl, pH 7.3, KOH, ~295 mOsm. If necessary, the osmolarity was adjusted by adding sucrose. Current-clamp recordings made with potassium gluconate-based solutions were corrected for a liquid junction potential of −10 mV by setting the reference voltage to −10 mV before seal formation.

Whole-cell recordings were obtained from granule cells in hippocampal slices using the "blind technique" and an SEC-05LX amplifier (standard headstage; NPI, Tamm, Germany) as described previously (Muller et al., 2005). Voltage and current signals were filtered at 8 kHz and 700 Hz, respectively, and digitized at 30 kHz with an ITC-16 interface (InstruTECH, Port Washington, NY) operated by TIDA (HEKA Elektronik, Lambrecht, Germany). Series resistance of the cells ranged between 20 and 30 MΩ and was estimated by bridge balancing after careful compensation of the pipette capacitance.

Hybrid-clamp recordings of the current underlying the fast afterhyperpolarization (I_{fAHP}) were performed as described previously (Dietrich et al., 2002). The switching frequency was set to 20–25 kHz. For a hybrid-clamp recording, the SEC-05LX amplifier operates in discontinuous single-electrode current clamp until an action potential triggered a mode switch to discontinuous single-electrode voltage clamp (dSEVC) for several seconds by a pulse generator (Master-8; A.M.P.I., Jerusalem, Israel). The mode switch was delayed by an interval (0.1–0.5 ms) chosen individually for every cell such that the switch coincided with that time point at which the falling phase of the action potential crossed approximately −40 mV. Because the cells were subsequently held at −40 mV in dSEVC mode, there was usually a small voltage step (±5 mV) associated with the mode switch that gives rise to a contaminating transient capacitive current. To correct for this current, we proceeded as follows. The amplitude of the voltage step during the switch was measured in the voltage trace. Then, an appropriately scaled current response to a −10 mV jump was aligned and subtracted from the hybrid trace.

Quantification of action potential duration. We induced action potentials by the injection of a depolarizing current such that the granule cells fired at <10 Hz. For an exact and reproducible quantification of the action potential duration, we proceeded as follows. We calculated two "reference" average action potentials of the control and of the triple toxin group in each case of five action potentials. We superimposed both reference action potentials and projected a vertical line from the time point of the peak of the control fAHP (see Fig. 1*B*, lower dot) to the triple-toxin action potential (see Fig. 1*B*, upper dot). All action potentials to be measured were aligned to the fast rising phase of both reference action potentials (as shown in Fig. 1*B*). The spike duration of the aligned action potentials was then measured at the voltage level defined by the latter dot.

Incubation with BKCh blockers and in low [Ca^{2+}]. Slices were incubated at room temperature in a small Petri dish and with bubbled 95% O_2/5% CO_2 ACSF containing albumin (0.1 mg/ml) and 10 μM paxilline, 1 μM charybdotoxin, or 1 μM iberiotoxin, a combination of all three blockers (triple toxin), or no blocker for ~1–4 h. After incubation, slices were transferred to an interface chamber perfused with ACSF (35 ± 0.5°C) (as described above) that, in addition, contained albumin (0.1 mg/ml) and 10 μM paxilline (10 μM), 45 nM charybdotoxin, or 60 nM iberiotoxin, all three blockers, or no blockers. There were no differences regarding action potential configuration or duration between nonincubated slices and slices incubated without blockers. For experiments in which action potentials were analyzed in low extracellular Ca^{2+} concentrations, slices were stored immediately after preparation in ACSF with low Ca^{2+} (1.5, 0.7, 0.5, and 0.2 mM). Reductions in extracellular Ca^{2+} were equimolarly compensated for by Mg^{2+}.

Conventional voltage-clamp recordings of Ca^{2+} currents

Whole-cell recordings of voltage-gated Ca^{2+} currents were either obtained from acutely isolated granule cells or from granule cells in slices. Because the results were not different between the two techniques, data were pooled.

For recording granule cells *in situ*, slices were prepared as described above, transferred to the stage of an upright microscope, and visualized using infrared video microscopy and differential interference contrast optics (E600 FN; Nikon Tokyo, Japan). Slices were perfused with ACSF at room temperature, which contained the following (in mM): 125 NaCl, 3 KCl, 2 $CaCl_2$, 2 $MgCl_2$, 20.3 $NaHCO_3$, 12 D-glucose, 0.0005 TTX, pH 7.4, gassed with 95% O_2/5% CO_2. Patch electrodes (3–5 MΩ) were filled with the following solution (in mM): 120 Cs^+-gluconate, 4 $MgCl_2$, 4 Na_2-ATP, 2 EGTA, 10 HEPES, 20 TEA-Cl, 15 CsCl, pH adjusted to 7.3 (CsOH), osmolarity adjusted to ~295 mOsm. Currents were recorded with an EPC-7 amplifier (HEKA Elektronik) operated by Igor Pro (WaveMetrics, Lake Oswego, OR). Series resistance ranged between 10 and 20 MΩ and was compensated electronically by 60–70%.

Isolated granule cells were prepared as described previously (Beck et al., 1997) and superfused with solution containing the following (in mM): 90 Na^+-methanesulfonate, 20 TEA, 5 4-aminopyridine, 2 $CaCl_2$, 2 $MgCl_2$, 3 KCl, 10 glucose, 26 $NaHCO_3^-$, 0.0005 TTX, pH 7.4, 315 mOsm osmolarity, gassed with 95% O_2/5% CO_2. Patch pipettes (4–5 MΩ) were filled with an intracellular solution containing the following (in mM): 87.5 Cs^+-methanesulfonate, 20 TEA, 0.5 $CaCl_2$, 5 $MgCl_2$, 5 BAPTA, 10 HEPES, 10 glucose, 10 Na_2-ATP, 0.5 Li_2-GTP, pH 7.2, 300 mOsm (adjusted with sucrose). Whole-cell recordings were obtained at room temperature, and currents were recorded using an EPC9 (HEKA Elektronik). Series resistance ranged between 8 and 15 MΩ and was compensated by 50–70%.

Cells were held at −75 mV, and Ca^{2+} currents were evoked every 10–30 s by an action potential-like command potential. The potential was instantaneously (or within 1 ms) stepped to +25 mV and returned to −75 mV using a linear ramp waveform with a duration of 5 ms. This protocol evoked a tail current that peaked approximately after half of the voltage ramp. All currents were leak corrected using either a +P/10 or a +P/5 strategy. To test the Ca^{2+} sensitivity of the peak of the tail currents,

Table 1. Biophysical properties of buffers and of Ca^{2+} as used for calculations and for simulation

	conc. (μM)	D ($\mu m^2/s$)	K_D (μM)	k_{on} ($M^{-1} s^{-1}$)
Ca^{2+}	0.05	220		
BAPTA	3000	110	0.22	4×10^8
Fixed buffer	500	0	50	1×10^8

In the case of Ca^{2+}, Conc. refers to concentration of free calcium, and in the case of BAPTA and fixed buffer, it refers to the total concentration. D, Diffusion coefficient; K_d, steady-state Ca affinity; k_{on}, calcium-binding rate. Values are according to Naraghi and Neher (1997) and Tsien (1980). Fixed buffer properties were assumed as by Nowycky and Pinter (1993).

extracellular Ca^{2+} was lowered from 2 mM to 1.5, 0.7, 0.5, and 0.2 mM. Reductions in extracellular Ca^{2+} were equimolarly compensated for by Mg^{2+}.

Calbindin-D_{28k} knock-out mice. The calbindin-D_{28k} null mutant mice used in this study were described previously (Airaksinen et al., 1997). We obtained mice from The Jackson Laboratory (Bar Harbor, ME), and homozygous knock-out mice were achieved by heterozygous breeding. All animals were genotyped by PCR using DNA samples extracted from tail tissue. The wild-type primers used were as follows: 5′-GCA AGT AAC TAA TGG CAT CG -3′ and 5′-TGC AGC GGC TAG TTT GAG AGT G-3′. The null mutant primers used were as follows: 5′-ACA TCG CAT CGA GCG AGC AC-3′ and 5′-AAG GCG ATG CGC TGC GAA TC-3′.

Numerical simulation of buffered Ca^{2+} diffusion around a single Ca^{2+} channel. Numerical simulations were performed to validate the linear approximation of microdomains as described previously (Muller et al., 2005). We were interested in the spatial and temporal development of free Ca^{2+} around the channel after its opening in the presence and absence of the buffer BAPTA. We consider a single Ca^{2+} channel that opens for 0.8 ms and is embedded in a planar membrane that limits a pseudo-infinitely large hemisphere (radius, 30 μm) around the channel that was divided into 30,000 shells. Within the first 600 nm from the origin, the shell size was constant at 0.06 nm, and the size of the following shells increased by 5% successively. In most preparations, a poorly mobile or even fixed Ca^{2+} buffer that will not wash out during the recording is found (Neher, 1995). For this reason, we incorporated a low amount of fixed Ca^{2+} buffer capacity ($\kappa_{fB} \sim 10$; Eq. 5) with Ca^{2+}-binding properties similar to those assumed in previous simulation studies (Nowycky and Pinter, 1993) (Table 1). The fixed Ca^{2+} buffer was homogeneously distributed in the diffusion volume. Diffusion coefficients and Ca^{2+} binding properties are summarized in Table 1. The maximum single-channel Ca^{2+} current (at physiological levels of divalent cations) was assumed to be 0.2 pA (Gollasch et al., 1992). Because we are interested in Ca^{2+} microdomains that develop during action potentials, we took into account the varying driving force of the single-channel current during the repolarizing phase of the action potential. Thus, the single-channel current is not square like; the channel opens and closes in a step-like manner, but the current steeply increases during the open time and reaches a value of 0.2 pA at the end of the opening. The time course of single-channel current amplitude was therefore empirically approximated with the following function (in pA): $0.2 \times (1 + \tanh(5 \times (t - 0.2)))/2$, where t (in milliseconds) is the time (see Fig. 6*A*, inset). Simulation starts at $t = 0$ ms and ends at 1.6 ms, and the channel closes abruptly at $t = 0.8$ ms. Before the simulation starts, buffers and Ca^{2+} are homogeneously distributed and have reached chemical equilibrium at resting Ca^{2+} concentration (50 nM). The differential equations were integrated using "Calcium Calculator (CalC)" software [version 4.9.8, freeware by V. Matveev (Matveev et al., 2004)]. This script-operated program uses the Crank–Nicholson differences scheme (one-dimensional) and an adaptive time-step method to maintain a given level of accuracy (<0.1%). Because CalC only offers full spherical geometry, we increased the single-channel current by a factor of 2, which yields identical results as simulating a hemisphere because of the complete symmetry. The correctness of the program was thoroughly checked against the transient analytical solutions of unbuffered Ca^{2+} diffusion and of buffered Ca^{2+} diffusion in case of a very mobile buffer (Crank, 1975; Pape et al., 1998). The output of the program was imported into Igor Pro for additional analysis and graphing.

Derivation of Equation 13, the formula used to estimate the distance r_{BK} between Ca^{2+} channel and BKCh. Ca^{2+} microdomains build up very rapidly after opening of a Ca^{2+} channel and reach values in the high micromolar range (Roberts, 1994). In the absence of any mobile Ca^{2+} buffer, a Ca^{2+} microdomain is described as the steady-state increase in Ca^{2+} above the resting concentration ($\Delta[Ca^{2+}]$), which is given by an inverse function of the distance (r) from a single Ca^{2+} channel (embedded in a planar membrane) according to the following equation (Crank, 1975):

$$\Delta[Ca^{2+}] = \frac{i_{Ca}}{4\pi \times F \times D_{Ca} \times r}. \quad (1)$$

In this equation, i_{Ca} is the single-channel current amplitude, F is the Faraday constant, and D_{Ca} is the diffusion coefficient of Ca^{2+}. Under some simplifying assumptions (see Results for details), the spatial extent of Ca^{2+} microdomains in the presence of BAPTA can be described well by a linear approximation yielding the following:

$$\Delta[Ca^{2+}]^{BAPTA} = \frac{i_{Ca}}{4\pi \times F \times D_{Ca} \times r} \times \exp\left(-\frac{r}{\lambda}\right), \quad (2)$$

with

$$\lambda := \sqrt{\frac{D_{Ca}}{k_{on} \times [BAPTA]_{free}}}, \quad (3)$$

(Neher, 1986, 1998), where k_{on} is the association rate constant of Ca^{2+} binding to BAPTA and $[BAPTA]_{free}$ is the concentration of BAPTA not bound to Ca^{2+} (Eq. 4). λ is a buffer length constant (in meters) that describes how the inhibitory effect of BAPTA on free Ca^{2+} increases with distance from the Ca^{2+} channel.

Now we consider a BKCh that is placed at a distance r_{BK} from the Ca^{2+} channel. Then, with $r = r_{BK}$, Equation 1 describes the increase in free Ca^{2+} seen by the BKCh in the absence of BAPTA ($\Delta[Ca^{2+}]_{BK}$). With $r = r_{BK}$, Equation 2 describes the free Ca^{2+} concentration at the BKCh in the presence of BAPTA ($\Delta[Ca^{2+}]_{BK}^{BAPTA}$).

Dividing Equation 2 by Equation 1 yields the following expression for the relative Ca^{2+} increase at the BKCh remaining in the presence of BAPTA:

$$\text{norm.}^{BAPTA}\Delta[Ca^{2+}]_{BK} := \frac{\Delta[Ca^{2+}]_{BK}^{BAPTA}}{\Delta[Ca^{2+}]_{BK}} = \exp\left(-\frac{r_{BK}}{\lambda}\right). \quad (13)$$

Other formulas and relationships

Ca^{2+}-free buffer concentration was calculated according to the law of mass action:

$$[buffer]_{free} = \frac{[buffer]_{total} \times K_{D,buffer}}{K_{D,buffer} + [Ca^{2+}]_{rest}}. \quad (4)$$

The Ca^{2+}-binding ratio was calculated as follows (Neher, 1995):

$$\kappa_{fB} = \frac{[fB] \times K_{D,fB}}{(K_{D,fB} + [Ca^{2+}]_{rest})^2}. \quad (5)$$

The diffusion time $t_{90\%}$ required to reach 90% of the steady-state Ca^{2+} concentration at a distance r from a permanently open single Ca^{2+} channel in the absence of buffers can be obtained from the following square-root relationship of diffusion (Crank, 1975):

$$0.9 = 1 - \text{erf}\left(\frac{r}{2\sqrt{D_{Ca}}\sqrt{t_{90\%}}}\right). \quad (6)$$

With an error function (erf) being ~0.1 at 0.0889 and $D_{Ca} = 2.2 \times 10^{-8}$ m^2/s (diffusion coefficient of free Ca^{2+} ions), it follows that:

$$t_{90\%} \approx 1.44 \times 10^{11} \times r^2. \quad (7)$$

The reduction in whole-cell Ca^{2+} currents evoked by mock action potentials caused by lowered extracellular Ca^{2+} concentration mainly reflects the reduction in single-channel current amplitude

The whole-cell Ca^{2+} current is related to the single-channel current by the following equation:

$$I_{Ca} = \sum_{k=1}^{N} i_{Ca,k}(t) \times P_{o,k}(t). \quad (8)$$

Here, N is the number of Ca^{2+} channels contributing to the whole-cell current, i_{Ca} is the single-channel current, and P_o is the open probability of channel i. The index, k, indicates that each of the N Ca^{2+} channels is allowed to have a different i_{Ca} and P_o (e.g., different subtypes of channels). i_{Ca} is time dependent because the driving force changes during the mock action potential. P_o is time, voltage, and Ca^{2+} dependent because gating properties of Ca^{2+} channels are time, voltage, and Ca^{2+} dependent. However, mock action potentials are short (~5 ms), and Ca^{2+}-dependent modulation of channel gating in granule cells develops with time constants >20 ms (Kohr and Mody, 1991). Thus, it seems reasonable to assume P_o primarily reflects voltage- and time- dependent gating and should primarily remain unaffected when the extracellular Ca^{2+} concentration is lowered. On the other hand, it can be expected that i_{Ca} will be reduced by lowering extracellular Ca^{2+}, $i_{Ca}{}^*$, because of a diminished occupancy of the channel pore by Ca^{2+} (Hille, 1992). Because the different Ca^{2+} channels bind Ca^{2+} with a similar affinity (Carbone and Lux, 1987; Church and Stanley, 1996), we assume that the fraction of i_{Ca} remaining in low Ca^{2+} solution, represented by $a \in [0,1]$, is similar between all of the N channels according to the following equation:

$$\frac{{}^*i_{Ca,k}}{i_{Ca,k}} = a,\ k = 1...N. \quad (9)$$

For the ratio "norm. I_{Ca}," under lowered extracellular Ca^{2+} concentrations (see Fig. 4*D*), it follows from Equations 8 and 9 that:

$$\text{norm.}I_{Ca} := \frac{{}^*I_{Ca}}{I_{Ca}} = \frac{\sum_{k=1}^{N} {}^*i_{Ca,k}(t) \times P_{o,k}(t)}{\sum_{k=1}^{N} i_{Ca,k}(t) \times P_{o,k}(t)} = \frac{\sum_{k=1}^{N} a \times i_{Ca,k}(t) \times P_{o,k}(t)}{\sum_{k=1}^{N} i_{Ca,k}(t) \times P_{o,k}(t)} = a. \quad (10)$$

In conclusion, under the above-mentioned assumptions, the reduction in norm.I_{Ca} equals the fraction of i_{Ca} that remains in low Ca^{2+} solution.

The percentage of reduction in whole-cell Ca^{2+} currents is a measure of the relative reduction in the increase in free Ca^{2+} concentration remaining at the BKChs in low Ca^{2+}, as follows:

$$\text{norm.}^{\text{low\_Ca}}\Delta[Ca^{2+}]_{BK} := \frac{\Delta^*[Ca^{2+}]_{BK}}{\Delta[Ca^{2+}]_{BK}} = \frac{{}^*i_{Ca}}{i_{Ca}} = \text{norm.}I_{Ca}, \quad (11)$$

with $\Delta^*[Ca^{2+}]_{BK}$ as the Ca^{2+} increase at the BKChs in low Ca^{2+}.

The following sigmoid function was used to interpolate the values in Figure 5*A*:

$$f(x) = \text{base} + \frac{\text{max}}{1 + e^{(\text{xhalf} - x)/\text{rate}}}, \quad (12)$$

with the following coefficients: base = 0.0016447; max = −0.00069526; xhalf = 0.30296; rate = 0.13025.

Equations were developed and checked in Derive for Windows 5.05 (Texas Instruments, Dallas, TX) and in Mathematica 5.1 (Wolfram Research, Champaign, IL). Fitting was performed in Igor Pro 5 for Windows (WaveMetrics)

Monte Carlo simulation of randomly distributed Ca^{2+} channels. The peak amplitudes of Ca^{2+} tail currents measured in granule cells (compare Fig. 4) ranged ~600 pA. Assuming a single-channel current of ~0.2 pA and an open probability of 0.15, this amplitude translates into ~20,000 voltage-gated Ca^{2+} channels on the granule cell surface. For one run of the simulations, we generated two series of 10,000 random numbers (Igor Pro) representing the spherical coordinates of Ca^{2+} channels on a hemisphere with a 5 μm radius. One series of numbers was equally distributed and ranged between 0 and 2π (φ), and the other equally distributed series of numbers (ϑ) ranged between 0 and 1 was converted to angles between 0 and π by the arccosine function to account for the variation of the perimeter of the sphere with ϑ. The BKCh was placed at angle (0, 0), and we determined the four smallest distances of the 10,000 distances from the Ca^{2+} channels to this BKCh. To simulate the collection of 27 granule cells (as used for calculating the data shown in Fig. 5*B*), we performed 30 runs of the simulation. For each run, we calculated the corresponding $-\ln(\text{norm.}\Delta[Ca^{2+}])$ curve for the four closest channels according to Equation 20 (with $n = 4$). We then averaged the 30 curves and calculated the SEM (see Fig. 5*B*). We also performed an analogous calculation with 10,000 runs to obtain the asymptotic curve. This asymptotic curve fell well within the SEM of the curve shown for 30 runs.

All of the drugs were from Sigma (Taufkirchen, Germany). Data are given as mean ± SEM. The level of statistical significance was set to $\alpha = 0.05$.

Results

BKChs are necessary for rapid repolarization of action potentials in granule cells

In hippocampal neurons, BKChs are activated by single action potentials, accelerate repolarization, and lead to a pronounced fAHP (Storm, 1987a; Shao et al., 1999). We tested the contribution of BKChs to action potential repolarization in hippocampal granule cells using established blockers of BKChs and whole-cell recordings. Paxilline (10 μM), charybdotoxin (1 μM), and iberiotoxin (1 μM) reduced the fAHP amplitude and significantly prolonged action potential duration in granule cells (Fig. 1). The combined application of the three blockers increased action potential duration to a similar degree as each blocker alone, suggesting that all inhibitors block the same type of channels. Together, and in agreement with previous findings in the CA1 region (Storm, 1987a; Shao et al., 1999), charybdotoxin- and iberiotoxin-sensitive BKChs are also critical for proper action potential repolarization in granule cells.

Endogenous Ca^{2+} buffers do not interfere with action potential repolarization

In the next series of experiments, we tested whether endogenous Ca^{2+} buffers, such as calbindin-D_{28k}, normally inhibit the activation of BKChs by action potentials. We tracked the activation of BKChs using hybrid-clamp recordings in whole-cell mode. In this way, it is possible to activate BKChs by action potentials and to simultaneously quantify the associated conductance change as a tail current amplitude [Dietrich et al. (2002), their Fig. 5]. To determine the effect of endogenous Ca^{2+} buffers on the I_{fAHP}, we took advantage of the fact that these buffers are strongly diluted during prolonged whole-cell recordings (>30 min) (Muller et al., 2005). If calbindin-D_{28k} or any other similarly mobile cytoplasmic Ca^{2+} buffer interferes with the activation of BKChs, we

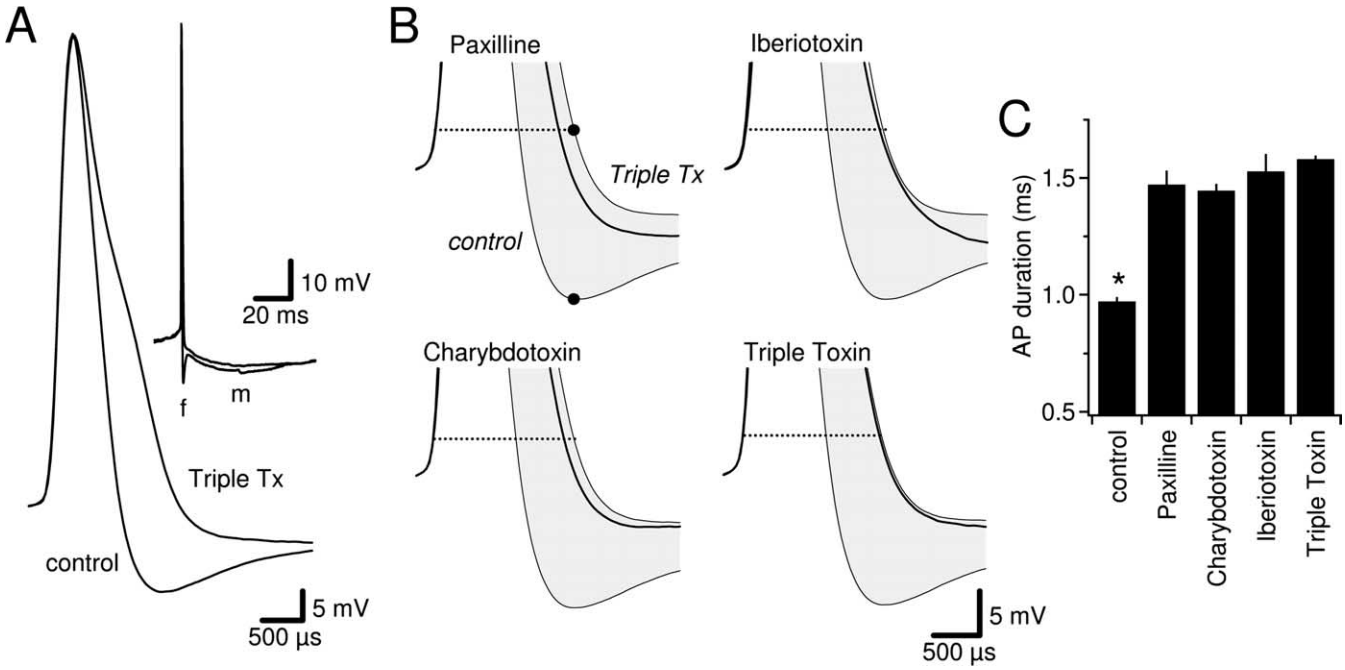

Figure 1. BKCh activation is required for rapid action potential repolarization in hippocampal granule cells. ***A***, Whole-cell current-clamp recordings of granule cells under control condition and after combined incubation in paxilline (10 μM), charybdotoxin (1 μM), and iberiotoxin (1 μM) (triple toxin). Notice the increase in spike duration and the reduction in the fAHP (f) in the presence of the blockers. The inset illustrates that the mAHP (m) is hardly affected by the incubation. ***B***, Action potentials (truncated for clarity) recorded in granule cells after incubation with 10 μM paxilline, 1 μM charybdotoxin, 1 μM iberioxin, and a mixture of the three BKCh blockers (Triple Tx). All four panels show individual action potentials recorded after incubation with the toxin as indicated and superimposed to averaged action potentials of the control and triple-toxin group. The dot in the control trace marks the peak of the fAHP. The time point of this peak was used to identify the voltage level (dotted line) at which we measured the action potential durations (see Materials and Methods for details). ***C***, Summary of action potential durations measured after incubation without blockers (control; $n = 9$) in paxilline ($n = 6$), charybdotoxin ($n = 4$), iberiotoxin ($n = 4$), and all three blockers ($n = 5$). The groups were significantly different (ANOVA) with pairwise differences between control and all blocker groups (asterisk) but with no difference between any of the blocker groups.

should observe an increase in I_{fAHP} caused by washout of Ca^{2+} buffers. However, I_{fAHP} remained constant during a recording period of >30 min, which dilutes calbindin-D_{28k} to <10% (Fig. 2*D*). As an additional test, we compared the action potential duration of granule cells from wild-type mice to those from calbindin-D_{28k}-deficient mice (Airaksinen et al., 1997). The properties of action potentials were not different between the two groups (Fig. 2*E*,*F*). Together, the data suggest that neither calbindin-D_{28k} nor any other mobile endogenous Ca^{2+} buffer influence the activation of BKChs by action potentials in hippocampal neurons.

Our previous work implied that calbindin-D_{28k} strongly reduces global Ca^{2+} signals [signals that spread over several micrometers (Augustine et al., 2003)] and localized Ca^{2+} signals down to a distance of ~200 nm from the source of entry (Muller et al., 2005). Thus, the lack of inhibition of BKCh activation by calbindin-D_{28k} indicates that Ca^{2+} ions diffuse <200 nm before they reach a BKCh. Ca^{2+} signals on such a restricted spatial scale are called Ca^{2+} microdomains. Ca^{2+} microdomains are steep submicroscopic Ca^{2+} concentration gradients around a Ca^{2+} channel or a cluster of channels that very rapidly equal steady state after opening of the channel and reach values in the high micromolar range (Roberts, 1994).

Millimolar BAPTA is required to inhibit BKCh activation by action potentials

To test the involvement of Ca^{2+} microdomains in the activation of BKChs, we compared the effects of the Ca^{2+} chelators BAPTA and EGTA on the repolarization of action potentials. If microdomain signaling is involved, Ca^{2+} ions diffuse only a brief period of time before they reach BKChs. Within this brief period, only a chelator with fast Ca^{2+} binding rates such as BAPTA (Tsien, 1980) is able to capture a significant fraction of Ca^{2+} ions (Roberts, 1993; Naraghi and Neher, 1997). Consistent with the involvement of microdomains, addition of a high concentration of the slow (Tsien, 1980) Ca^{2+} chelator EGTA (10 mM) to the solution in the patch pipette did not prolong action potentials (Fig. 3*A*,*C*). In contrast, as illustrated in Figure 3, *A* and *B*, spike duration clearly increased in a concentration-dependent manner when cells were loaded with BAPTA. A concentration of 10 mM BAPTA prolonged action potentials slightly less than pharmacological blockade of BKChs by toxins (compare Fig. 1). The insensitivity of BKCh activation to EGTA is in line with previous findings in different types of cells and qualitatively indicates a close association between a BK and a Ca^{2+} channel (Robitaille et al., 1993; Prakriya and Lingle, 2000; Protti and Uchitel, 1997; Storm, 1987b).

Linear approximation of Ca^{2+} diffusion in microdomains allows the estimation of the diffusional distance between BK and Ca^{2+} channels

The concentration dependence of the effect of BAPTA on the action potential repolarization can be used to estimate the mean diffusional distance between Ca^{2+} and BKChs. The linear approximation of Ca^{2+} diffusion within Ca^{2+} microdomains describes the relative increase in Ca^{2+} above resting concentration at a certain distance from the source of entry in the presence of a Ca^{2+} buffer such as BAPTA (Naraghi and Neher, 1997; Neher, 1998). According to this approximation, the local Ca^{2+} concentration at a BKCh placed at the distance r_{BK} from a Ca^{2+} channel

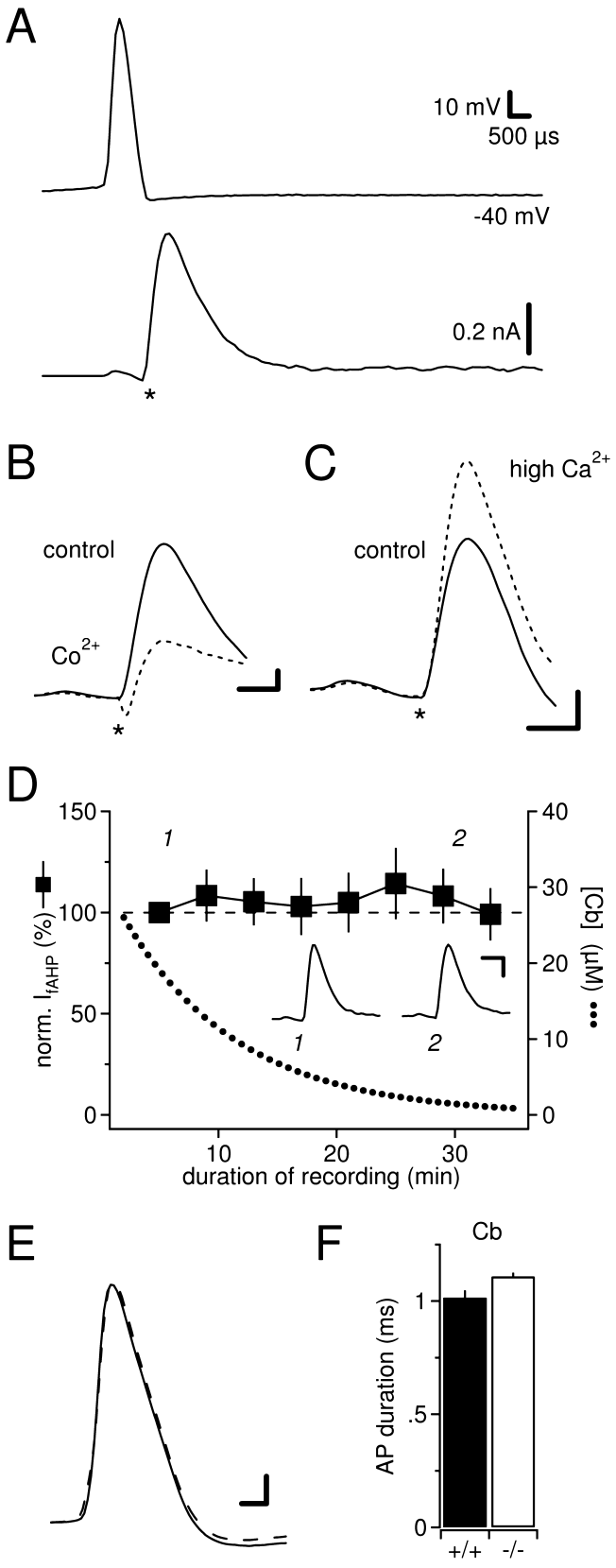

Figure 2. Action potential-mediated activation of BKChs is not influenced by mobile endogenous Ca^{2+} buffers. ***A***, Example of an original hybrid-clamp recording trace. Voltage (top trace) and current (bottom trace) are recorded in parallel. The recording starts at the left in current-clamp mode and is switched after the action potential (indicated by the asterisk) to voltage-clamp mode. Immediately after the mode switch, there is a fast and transient outward current (I_{fAHP}). This outward current usually produces the fAHP and reflects the activation of BK and other channels by the preceding action potential. The action potential was evoked by a rectangular current injection in current-clamp mode. This injection starts several hundred milliseconds before the action potential and is therefore not depicted on the graph. ***B***, I_{fAHP} is Ca^{2+} sensitive. Example traces of leak-corrected (see Materials and Methods) action potential tail currents before and after 30 min perfusion of ACSF in which Ca^{2+} is replaced by the Ca^{2+} channel antagonist Co^{2+}. As expected, I_{fAHP} amplitude decreased to 40 ± 4% ($n = 4$). Calibration: 500 μs, 0.1 nA. ***C***, I_{fAHP} is not fully activated by a single action potential. Perfusion of ACSF with increased [Ca^{2+}] (4 mM Ca^{2+}, 0.3 mM Mg^{2+}) for 20 min potentiated leak-corrected tail currents to 142 ± 15% ($n = 5$). This shows that BKChs are not saturated by Ca^{2+} subsequent to a single action potential and, accordingly, that I_{fAHP} should increase if inhibition by endogenous buffers is removed (see ***D***). Calibration: 500 μs, 0.1 nA. ***D***, Time course of action potential tail current amplitude (I_{fAHP}), recorded as illustrated in ***A***, during prolonged whole-cell recordings from granule cells ($n = 8$). I_{fAHP} amplitudes were normalized to the amplitude measured in the first 5–7 min after gaining whole-cell access. Note, that I_{fAHP} remains stable for >30 min (left axis). This is despite the significant drop in intracellular calbindin-D_{28k} concentration caused by the whole-cell perfusion (right axis). The dotted line indicates the time course of dilution of cellular calbindin-D_{28k} content and was taken from our previous work (Muller et al., 2005). The results indicate that neither calbindin-D_{28k} nor any other similarly mobile buffer normally exert a suppressing effect on the activation of BKChs. Inset, Example traces taken from time points indicated by the small numbers. Calibration: 1 ms, 0.2 nA. ***E***, Action potential properties are identical between wild-type (full line) and calbindin-D_{28k} null mutant mice (dashed trace). Calibration: 250 μs, 10 mV. ***F***, Quantification of action potential duration in wild-type ($n = 6$) and calbindin-D_{28k}-deficient ($n = 8$) mice. Action potential durations are not different between the two groups.

is given by the following equation (see Materials and Methods for details):

$$\text{norm.}^{\text{BAPTA}}\Delta[Ca^{2+}]_{BK} := \frac{\Delta[Ca^{2+}]_{BK}^{BAPTA}}{\Delta[Ca^{2+}]_{BK}} = \exp\left(-\frac{r_{BK}}{\lambda}\right), \quad (13)$$

where $\Delta[Ca^{2+}]_{BK}^{BAPTA}$ and $\Delta[Ca^{2+}]_{BK}$ represent the differential increase in free Ca^{2+} at the BKCh in the presence and absence of BAPTA and λ is a buffer-length constant that describes how the inhibitory effect of BAPTA on free Ca^{2+} increases with the distance from the Ca^{2+} channel (Neher, 1986; Naraghi and Neher, 1997).

Principally, from Equation 13, the mean distance, r_{BK}, which Ca^{2+} ions diffuse from Ca^{2+} to BKChs, can be calculated provided that λ as well as norm.$^{\text{BAPTA}}\Delta[Ca^{2+}]_{BK}$ are known. λ can easily be computed (Eqs. 3, 4) from the well known biophysical properties of BAPTA and Ca^{2+} (Tsien, 1980). It is less straightforward to assess norm.$^{\text{BAPTA}}\Delta[Ca^{2+}]_{BK}$ because it is not possible to directly measure Ca^{2+} concentrations at the required spatial and temporal resolution (tens of nanometers, submillisecond range). Here, we use an alternative calibration procedure to obtain information on this local Ca^{2+} concentration in four steps, explained as follows, in brief: (1) we measured how the action potential duration increases when decreasing the local Ca^{2+} concentration at the BKCh (norm.$^{\text{low\_Ca}}\Delta[Ca^{2+}]_{BK}$) by perfusion of low extracellular Ca^{2+} concentration; (2) we estimated how the single-channel Ca^{2+} current (i_{Ca}) reduces when perfusing low extracellular Ca^{2+} concentration; (3) we used the reduction in i_{Ca} as a measure of norm.$^{\text{low\_Ca}}\Delta[Ca^{2+}]_{BK}$ and constructed a calibration curve (from the data obtained in steps 1 and 2) that provides the corresponding value of norm.$\Delta[Ca^{2+}]_{BK}$ for any given AP duration; (4) with the help of this curve, we translate the AP durations measured in the presence of BAPTA (see Fig. 5*A*) into the corresponding values of norm.$^{\text{BAPTA}}\Delta[Ca^{2+}]_{BK}$.

←

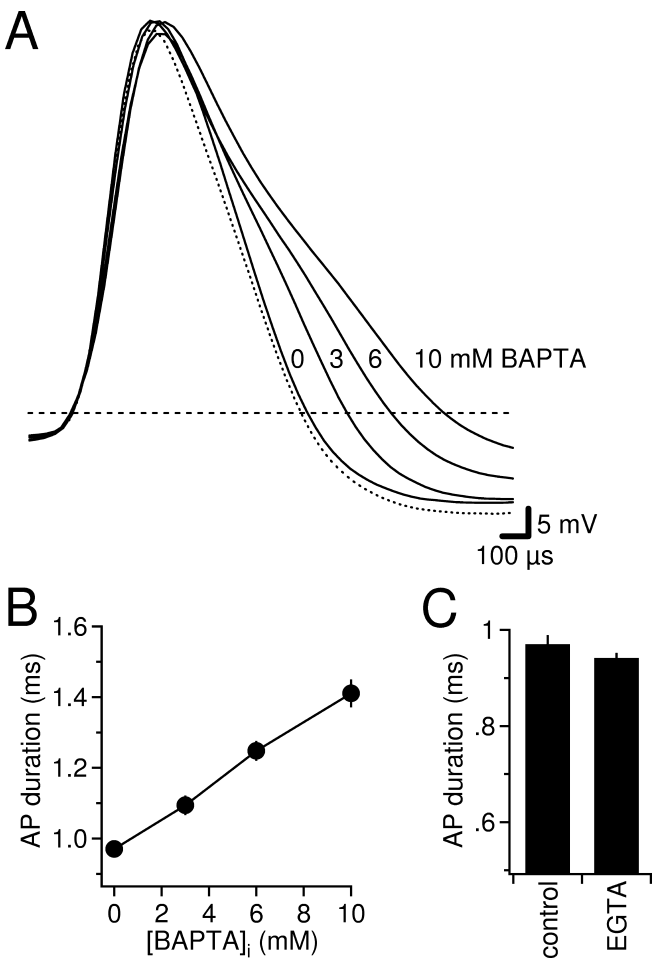

Figure 3. BKCh activation by action potentials involves Ca^{2+} microdomain signaling. ***A***, Action potentials in granule cells recorded with pipettes containing 0, 3, 6, and 10 mM of the fast Ca^{2+} chelator BAPTA. The action potential duration increased in a comparable manner as by application of BKCh blockers. A concentration of 10 mM EGTA did not affect the kinetics of action potentials (dotted trace). ***B***, Concentration–duration relationship for BAPTA [action potential (AP)]. No buffer, $n = 9$; 3 mM, $n = 10$; 6 mM, $n = 8$; 10 mM, $n = 9$. ***C***, Quantification of action potential duration in cells measured with pipette solution containing no Ca^{2+} chelator or 10 mM EGTA ($n = 4$). A concentration of 10 mM EGTA does not effect on spike duration.

Calibrating the prolongation of action potentials by BAPTA on the prolongation induced by low extracellular Ca^{2+}

In detail, we performed the following experiments. (1) We lowered the extracellular Ca^{2+} concentrations and kept the totaldivalent cation concentration constant by substitution of equimolar Mg^{2+} to avoid divalent screening effects. Figure 4, *A* and *B*, depicts the increase in spike duration when extracellular Ca^{2+} was lowered from 2 mM to 1.5, 0.7, 0.5, and 0.2 mM. (2) I_{Ca} was measured in whole-cell voltage-clamp mode and evoked by mock action potentials as command potential (Fig. 4*C*). Figure 4*D* illustrates the concentration-dependent decrease in I_{Ca} when lowering the extracellular Ca^{2+} concentration. As outlined in Materials and Methods, under the conditions used here, the fraction of I_{Ca} remaining in low extracellular Ca^{2+} (norm.I_{Ca}) is a measure of the fraction of the single-channel current amplitude remaining in the same concentration. (3) Because microdomain Ca^{2+} scales proportionally to i_{Ca} (Eqs. 1, 2), norm.I_{Ca} is also a measure of the relative action potential-triggered increase in free Ca^{2+} concentration remaining at the BKChs in low [Ca^{2+}]. Therefore, the following equation is satisfied:

$$\text{norm.}^{\text{low\_Ca}}\Delta[Ca^{2+}]_{BK} = \text{norm.}I_{Ca}, \quad (14)$$

and we can construct a calibration curve by replacing the scaling of the abscissa in Figure 4*B* with the ordinate of Figure 4*D* (i.e., we plot the action potential duration measured at various extracellular Ca^{2+} concentrations versus the corresponding norm.$^{\text{low\_Ca}}\Delta[Ca^{2+}]_{BK}$ values (Fig. 5*A*, data pairs taken from Fig. 4*B*,*D*). The data points were interpolated with a sigmoid function (dashed line; see Materials and Methods). For any given increment in spike duration, the corresponding relative decrease in the local Ca^{2+} concentration at the BKCh can be deduced from this curve. (4) In particular, this plot yields the values of norm.$^{\text{BAPTA}}\Delta[Ca^{2+}]_{BK}$ that gave rise to the increased action potential durations in the presence of different concentrations of intracellular BAPTA (Fig. 3). We used the inverse of the sigmoid function to compute the values of norm.$^{\text{BAPTA}}\Delta[Ca^{2+}]_{BK}$ corresponding to the spike durations recorded with 0, 3, 6, and 10 mM BAPTA (Fig. 5*A*, see example arrow).

Graphical approach to infer the diffusional distance of Ca^{2+}

Taking advantage of Equation 13, we developed a graphical approach to estimate the value of r_{BK} based on the concentration-dependent inhibitory effect of BAPTA. Rearranging Equation 13 yields a linear function of the reciprocal buffering length constant ($1/\lambda$) with a slope of r_{BK} as follows:

$$-\ln(\text{norm.}\Delta[Ca^{2+}]_{BK}) = r_{BK} \times \frac{1}{\lambda}. \quad (15)$$

Thus, when BKChs are only activated by Ca^{2+} channels that are placed at a distance of r_{BK}, the plot of $-\ln(\text{norm.}^{\text{BAPTA}}\Delta[Ca^{2+}]_{BK})$ versus $1/\lambda$ should be a straight line through the origin. The slope of that line represents r_{BK}. The values of norm.$^{\text{BAPTA}}\Delta[Ca^{2+}]_{BK}$ were obtained from the calibration plot in Figure 5*A* as described above, and λ was calculated according to Equation 3, Equation 4, and using published parameters summarized in Table 1 (yielding $\lambda = 15$, 10.6, and 8.2 nm for 3, 6, and 10 mM BAPTA respectively). As illustrated in Figure 5*B*, the data could be well fitted by a line crossing the origin with a slope of $r_{BK} = 12.7$ nm. This value is also obtained if we fit our data with a formula derived from the full model (from Eq. 20, supplemental Fig. 1, available at www.jneurosci.org as supplemental material). Even an unconstrained linear fit yields a very similar estimate of 13.5 nm (data not shown). Thus, there must be a very close spatial association between BKChs and voltage-gated Ca^{2+} channels such that Ca^{2+} ions diffuse, on average, only ~13 nm.

It is important to note that plotting $-\ln(\text{norm.}^{\text{BAPTA}}\Delta[Ca^{2+}]_{BK})$ versus $1/\lambda$ generates a line only when BKChs exclusively sense Ca^{2+} from a source (or sources) located at r_{BK} and not from additional Ca^{2+} sources at other distances. If additional remote channels contributed to the activation of the BKCh, then the resulting graph would be a curve that starts from the origin with a steep slope and that converges into a more shallow line (constant slope) as $1/\lambda$ increases (see Appendix). This case is illustrated by the dashed line that signifies how the plot would look if BKChs were activated by four Ca^{2+} channels placed at 12.7, 50, 60, and 70 nm (according to Eq. 20) (Fig. 5*B*,*C*). The initial slope of this curve is steeper because a low BAPTA concentration (low $1/\lambda$ values) can already cause a significant reduction in

$\Delta[Ca^{2+}]_{BK}$ by capturing Ca^{2+} from remote sources. When BAPTA concentration (and $1/\lambda$) is increased further, the contribution of more remote sources is shut off successively, and the slope of the curve flattens. Finally, when the BAPTA concentration is sufficiently high such that BKChs sense only Ca^{2+} from the closest source at r_{BK}, the curve continues as a line with the slope r_{BK}.

It can be shown that even when several channels contribute to the local Ca^{2+} concentration at the BKCh, the graphical analysis of a plot, as shown in Figure 5*B*, yields estimates of the distance of the closest Ca^{2+} channel, of the fraction of the local Ca^{2+} that this closest channel contributes, and of the total number of Ca^{2+} channels that participate in activating the BKCh (see Appendix).

Random placement of channels cannot explain the colocalization

We next asked whether such a tight colocalization may also result from a random placement of Ca^{2+} channels on the granule cell surface. Based on the amplitudes of Ca^{2+} currents measured above, we estimated the mean number of Ca^{2+} channels in granule cells (see Materials and Methods for details) and performed a simple Monte Carlo simulation of the distribution of channels. Based on the random distribution of the four closest Ca^{2+} channels, we calculated the corresponding $-\ln(\text{norm.}\Delta[Ca^{2+}])$ plot according to Equation 20. These simulations (Fig. 5) clearly show that the observed increase in action potential duration by BAPTA can hardly be the result of random channel distributions.

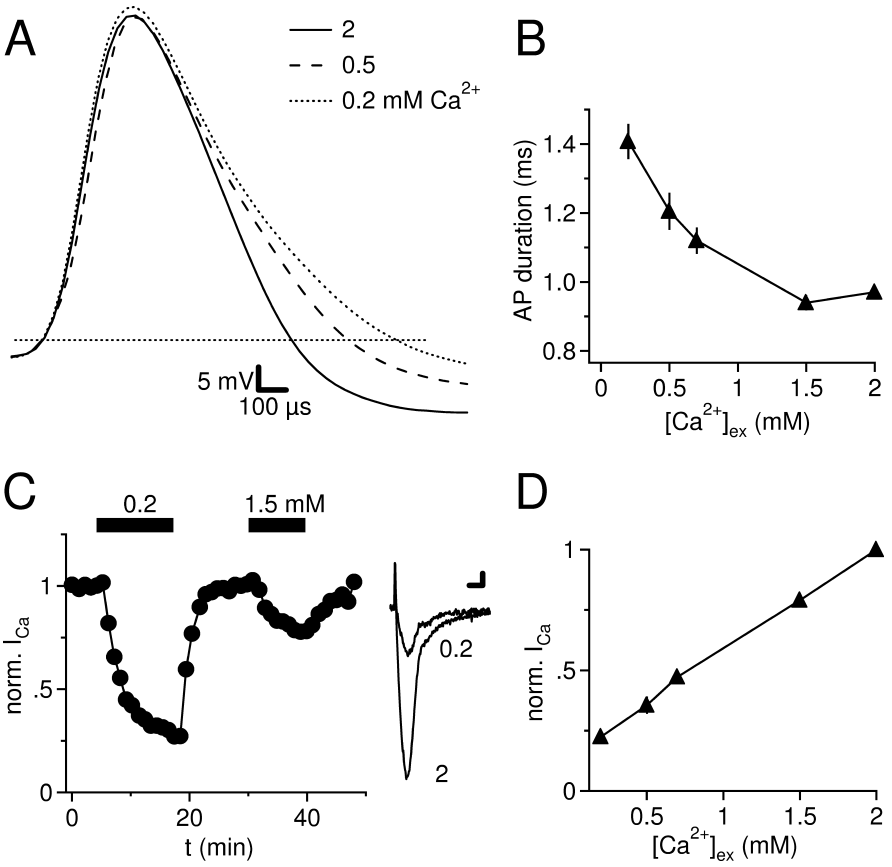

Figure 4. Sensitivity of action potential duration and Ca^{2+} entry to changes in extracellular Ca^{2+}. ***A***, Action potentials broaden after perfusion of low extracellular Ca^{2+}. Traces are taken from cells incubated in and perfused with 2 mM (control), 0.5 mM, and 0.2 mM extracellular Ca^{2+} (see Materials and Methods). ***B***, Ca^{2+} sensitivity of the action potential duration. Extracellular Ca^{2+} concentration was reduced to decrease Ca^{2+} microdomains by a reduction in the single-channel Ca^{2+} current (see text for details). 2 mM, $n = 9$; 1.5 mM, $n = 7$; 0.7 mM, $n = 5$; 0.5 mM, $n = 4$; 0.2 mM, $n = 6$. ***C***, Mock action potentials were used as command potential to evoke pharmacologically isolated Ca^{2+} tail currents in voltage-clamp mode. Left, Example time course of the normalized Ca^{2+}-tail current amplitude (in 2 mM Ca^{2+}). Bars indicate perfusion of lower extracellular Ca^{2+} concentrations as indicated. A slight rundown during this experiment (20% over 50 min) was corrected by normalizing on an exponential function fitted to points of baseline periods. Right, Example traces of Ca^{2+}-tail currents recorded in 2 and 0.2 mM Ca^{2+}. Calibration: 2 ms, 50 pA. ***D***, Ca^{2+} sensitivity of voltage-gated Ca^{2+} channels recorded in whole-cell voltage-clamp mode. In each experiment, the amplitude of the tail current was normalized on the amplitude measured in the presence of 2 mM extracellular Ca^{2+} (1.5 mM, $n = 6$; 0.7 mM, $n = 7$; 0.5 mM, $n = 9$; 0.2 mM, $n = 5$).

Validation of the linear approximation of Ca^{2+} diffusion by numerical simulations

In the above analysis, we rely on the accuracy of the linear approximation of Ca^{2+} diffusion in microdomains, which makes several simplifying assumptions (Naraghi and Neher, 1997; Neher, 1998), such as immediate steady state of free Ca^{2+} concentration during a square-like single-channel current and negligible buffer depletion. We used numerical simulations of buffered diffusion of Ca^{2+} to verify that this model also holds in a more physiological scenario incorporating a time-dependent single-channel Ca^{2+} current and the presence of fixed Ca^{2+} buffers that compete with BAPTA (see Materials and Methods for details).

In agreement with previous studies (Simon and Llinas, 1985; Roberts, 1994) and with analytical approaches (Naraghi and Neher, 1997; Pape et al., 1998), the free Ca^{2+} at a distance of 15 nm, and to a slightly lesser degree at 50 nm, closely follows the time course of the tail-like single-channel current and nearly approaches the steady-state concentration before the channel closes (Fig. 6*A*, arrowheads). Figure 6, *A* and *B*, shows that BAPTA effectively reduces the free Ca^{2+} concentration at 15 and 50 nm to ~40 and ~5% of the value reached without BAPTA, respectively. Because of the very fast Ca^{2+}-binding rate of BAPTA, the free Ca^{2+} concentration in the presence of the buffer still closely follows the time course of unbuffered Ca^{2+} concentration (Fig. 6*A*), and the inhibition produced by BAPTA commences nearly instantaneously (Fig. 6*B*). The approximation of buffered Ca^{2+} microdomain diffusion linearizes around the concentration of Ca^{2+}-bound buffer. It was therefore important to verify that the deviations in this parameter are insignificant (Fig. 6*C*). Together, the model of linear approximation of buffered Ca^{2+} diffusion used for estimating the distance between BK and Ca^{2+} channels describes the inhibition of free Ca^{2+} concentration in the immediate vicinity of a Ca^{2+} channel during an action potential very well (Fig. 6*D*).

Discussion

The main results of the present study is that BKChs are tightly colocalized with voltage-gated Ca^{2+} channels such that Ca^{2+} ions have to diffuse, on average, only ~13 nm after entering the cell before they bind to BKChs. The operation of BKChs by nanodomains of single Ca^{2+} channels provides several unique ad-

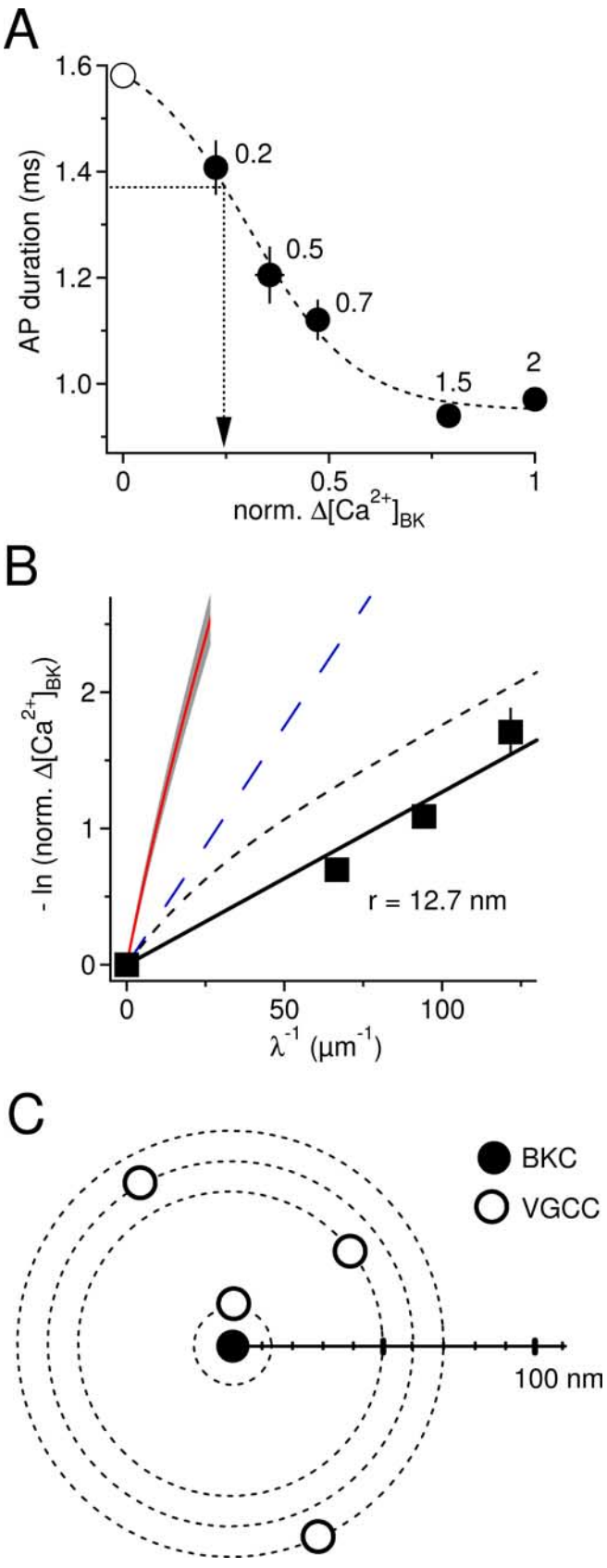

Figure 5. The mean diffusional distance between a BKCh and a Ca^{2+} channel is ~13 nm. ***A***, Inferring the reduction in local Ca^{2+} increase at BKChs by BAPTA based on the action potential broadening induced by BAPTA. Data points from Figure 4, *B* and *D*, were combined according to the Ca^{2+} concentration at which they have been measured. Then action potential durations were plotted versus norm.I_{Ca}. Norm.I_{Ca} was renamed in norm.$\Delta[Ca^{2+}]_{BK}$ because it represents a measure of the local Ca^{2+} concentration at the BKChs (see text for details). The values were fitted by a sigmoid function. The action potential durations measured in the presence of different concentrations of BAPTA (as shown in Fig. 3*B*) were translated into the corresponding relative reductions in local Ca^{2+} at BKChs by inserting them into the inverse of the sigmoid function. This procedure is illustrated graphically (arrow) for an action potential duration measured with 10 mM BAPTA. The arrow marks the inferred value of norm $^{BAPTA}\Delta[Ca^{2+}]_{BK}$ at the abscissa. The open circle denotes the action potential duration measured after incubation with the three BKCh blockers standing for the condition of no activation of BKChs (functionally equivalent to norm. $^{BAPTA}\Delta[Ca^{2+}]_{BK} = 0$). ***B***, Plot of the ln-transformed norm. $\Delta[Ca^{2+}]_{BK}$ values, as obtained in ***A***, versus the corresponding inverse buffer length constant, λ^{-1}, associated with the respective BAPTA concentration Equation 3. The data points were fitted with a line through the origin and a slope of 12.7 nm. The dashed line signifies how the plot would look if BKChs were activated by four Ca^{2+} channels placed at 12.7, 50, 60, and 70 nm (according to Eq. 20). The blue dashed line denotes the situation when *n* Ca^{2+} channels are placed at a distance of 35 nm. The red line signifies the ln-transformed norm.$\Delta[Ca^{2+}]_{BK}$ values that would be obtained if Ca^{2+} channels were randomly distributed on the cell surface. The red line and the gray area represent the average and the SEM of 30 runs of a Monte Carlo simulation randomly placing 20,000 channels on a granule cell, respectively. The average converged within several thousand runs into a curve that fell into in the gray area. ***C***, Scheme of the geometric arrangement of BK and Ca^{2+} channels that was used to calculate the dashed line in ***B***. One BKCh is surrounded by four voltage-gated Ca^{2+} channels placed at 12.7, 50, 60, and 70 nm.

vantages, as discussed below. This functional colocalization was determined by a novel approach based on a linear approximation of buffered Ca^{2+} diffusion in microdomains (Neher, 1986; Stern, 1992; Naraghi, 1997).

This approach involved the quantitative analysis of the effect of the Ca^{2+} chelator BAPTA on the repolarization phase of action potentials, which we have shown to be potently shaped by BKChs. When we plotted the ln-transformed normalized local Ca^{2+} versus the inverse buffer length constant ($1/\lambda$), the points could be well fitted with a line through the origin and a slope of 12.7 nm. Because our approach involves a calibration of the Ca^{2+}-dependent response (action potential duration) on defined relative reductions of the local Ca^{2+} increases (obtained by lowering extracellular Ca^{2+}), it does not require estimates of the absolute local Ca^{2+} concentration at the target. Therefore, it should prove useful for Ca^{2+}-dependent processes other than activation of BKChs as well.

How precise is this estimate of 13 nm diffusional distance? The data shown in Figure 5*B* potentially result from the summation of responses on two levels. First, the local Ca^{2+} at a single BKCh could be the sum of two Ca^{2+} channels very close to each other. If, for example, two Ca^{2+} channels are placed at 11 and 15 nm distances from the BKCh, then a plot would result that is indistinguishable from our results within the range of experimental accuracy. However, when the closest channel of such a cluster is located at a distance ≤8 nm, then the reduction in the Ca^{2+} elevation caused by 10 mM BAPTA would be detectably smaller than what we observed. Likewise, when the most remote channel is placed at a range ≥18 nm, the curve would clearly bend and pass into the asymptotic linear course in the presence of ≥3 mM BAPTA. Thus, several Ca^{2+} channels could contribute to the activation of a BKCh if they were placed in the range of ~8–18 nm away from the BKCh. However, given that in hippocampal neurons BKCh openings seemed to follow sparse openings of Ca^{2+} channels (Marrion and Tavalin, 1998), it appears more likely that they are operated by single Ca^{2+} channels.

Second, BKCh activation was monitored in whole-cell recordings that represent the summed response of hundreds of BKChs. If each BKCh is operated by a single Ca^{2+} channel, then the respective −ln plots of the fractional local Ca^{2+} will be linear

functions of $1/\lambda$ for all participating channels. The slopes of those individual plots do not have to be identical but could vary around the arithmetical average of 13 nm. However, because the physical extent of an ion channel protein is ~8 nm (Hille, 1992), the range of possible distances between individual BK and Ca^{2+} channels that yields an average of 13 nm has to be ~8–18 nm (assuming a symmetrical distribution). Such a constant spacing is suggestive of a physical link between the two channels that could potentially be mediated by β-catenin (Lesage et al., 2004).

Together, our results clearly indicate a tight association between BK and Ca^{2+} channels, such that the mean diffusional distance for Ca^{2+} ions is as short as ~8–18 nm. The most parsimonious explanation for this scenario is that each BKCh is operated by a Ca^{2+} nanodomain, a microdomain of a single Ca^{2+} channel (Augustine et al., 2003).

The nanodomain operation of BKChs imparts several unique functional advantages that are all connected to the spatial and temporal spread of this very local Ca^{2+} signaling. First of all, the short mean diffusional distance of Ca^{2+} ions assures that BKChs are activated very rapidly and are able to effectively contribute to the repolarization of an action potential. This is in striking contrast to other Ca^{2+} activated K^+ channels, such as small conductance Ca^{2+}-activated K^+ (sK) channels, which open as rapid as BKChs (Xia et al., 1998; Ha et al., 2004); however, they do not contribute to repolarization, but instead produce a slower AHP that peaks with a delay of ~5 ms (Sah, 1996). The reason for the different AHP kinetics may be that Ca^{2+} ions need only ~0.03 ms to reach ~90% of the steady-state concentration at a distance of 13 nm (nanodomain), whereas at a distance of 200 nm (microdomain), the time to reach this level is strongly prolonged to ~5 ms (Eq. 7).

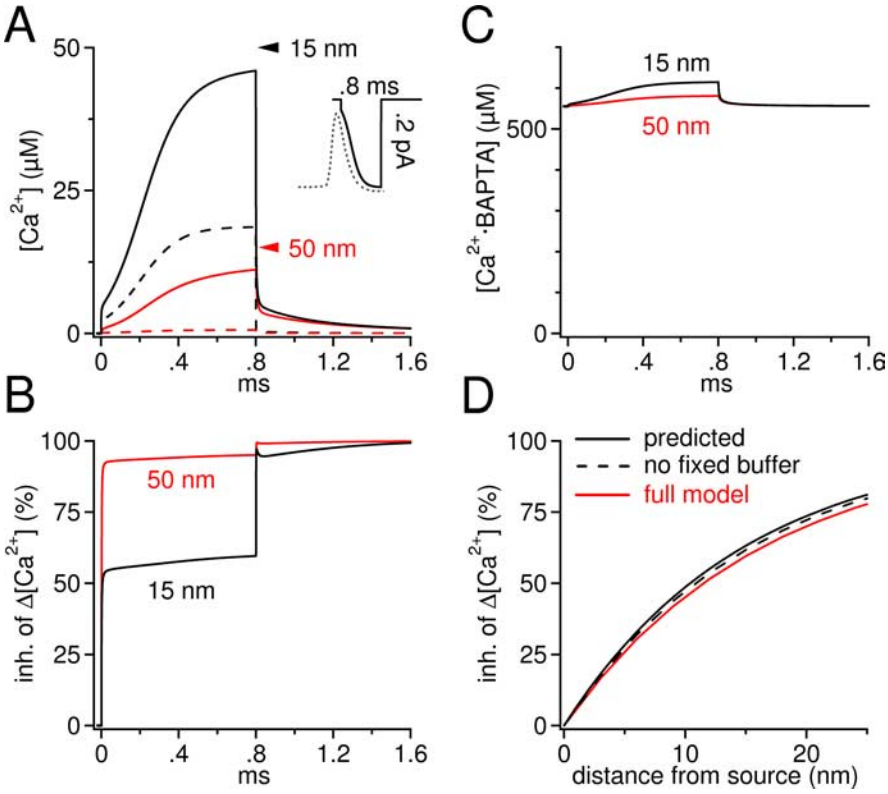

Figure 6. Numerical simulation of buffered Ca^{2+} diffusion around a single Ca^{2+} channel. ***A***, Time course of free Ca^{2+} during and after a 0.8 ms opening of a single Ca^{2+} channel in the absence (continuous lines) and in the presence (dashed lines) of 3 mM BAPTA. The inset shows the simulated tail-like single-channel Ca^{2+} current. BAPTA is very effective in reducing the free Ca^{2+} concentration even very close to the source (15 nm). Note that after the closure of the channel, Ca^{2+} drops below the threshold for activation of BKChs [~2 μM at −40 mV (Magleby, 2003)] within ~400 μs. Arrowheads denote the steady-state concentration of free Ca^{2+} reached at 15 and 50 nm if the channel remained open and if Ca^{2+} were diffusing in an unlimited hemisphere. ***B***, Time course depicting the percentage of inhibition of the increase in Ca^{2+} above resting Ca^{2+} ($\Delta[Ca^{2+}]$) caused by 3 mM BAPTA at 15 and 50 nm. Curves were calculated from the respective control and buffer time courses of free Ca^{2+}, as shown in ***A***. It is clearly seen that the inhibitory effect of BAPTA develops nearly instantaneously in response to changes in Ca^{2+} entry. This implies that the time course of Ca^{2+} at the BKChs is hardly altered by the addition of BAPTA (i.e., that BAPTA proportionally and time independently reduces the free Ca^{2+} concentration as predicted by the linear approximation). ***C***, Time course of the concentration of Ca^{2+}-bound BAPTA. At rest (50 nM Ca^{2+}), ~550 μM BAPTA has bound Ca^{2+}. The relative change in Ca^{2+}-bound BAPTA is small, even as close as 15 nm at the Ca^{2+} channel. ***D***, The linear approximation yields excellent results in predicting the inhibitory effect of BAPTA. The radial gradient shows the percentage of inhibition of the increase in Ca^{2+} above resting Ca^{2+} ($\Delta[Ca^{2+}]$) caused by 3 mM BAPTA. The red line depicts the inhibition caused by BAPTA, as revealed by the full model used in ***A–C***. The black line indicates the predicted effect of 3 mM BAPTA according to the linear approximation of Ca^{2+} microdomains (Eq. 13). Half of the small deviation is caused by the presence of fixed Ca^{2+} buffers (see Materials and Methods) that compete with BAPTA for binding of Ca^{2+} (dashed line).

Second, at a distance of 13 nm from a Ca^{2+} channel, the free Ca^{2+} concentration also drops back to resting levels within microseconds after closure of the Ca^{2+} channel (Fig. 6) (Roberts, 1994; Naraghi and Neher, 1997). Thus, the period of activation of BKChs is given by the very brief open time of Ca^{2+} channels during an action potential [<1 ms (Lee and Elmslie, 1999)] and prevents BKChs from suppressing repetitive firing. In contrast, the kinetics of Ca^{2+}-activated currents operated by a more remote regimen will primarily dependent on the removal of Ca^{2+} by sequestering mechanisms that typically requires several hundred milliseconds (Helmchen et al., 1996).

Third, there is a multitude of intracellular processes that are triggered by elevations in intracellular Ca^{2+}. Still, single action potentials do not usually trigger many of these processes, but they consistently lead to activation of BKChs. This selectivity of BKCh activation partially results from the steep spatial gradient of Ca^{2+} nanodomains. Ca^{2+} nanodomains reach high micromolar concentrations only very close to the source (the Ca^{2+} channel), and at a few hundred nanometers off of the source, the free Ca^{2+} concentrations only reach the low or submicromolar range. Therefore, Ca^{2+}-binding partners placed far away from the source have much less chances to bind sufficient Ca^{2+} ions to be activated after single action potentials.

Fourth, the restricted spatial extent of Ca^{2+} nanodomains also confers reliability on BKCh activation. The actual concentration of Ca^{2+}-binding partners competing with BKChs can change drastically. For example, in response to ischemia and neuronal activity, certain neurons strongly increase the expression of Ca^{2+}-binding proteins such as calbindin-D_{28k} (Lowenstein et al., 1991; Batini et al., 1993; Arnold and Heintz, 1997). If competing Ca^{2+}-binding partners strongly increase in concentration, activation of BKChs could decrease concomitantly. However, considering

that BAPTA binds Ca^{2+} two to four times faster than endogenous Ca^{2+}-binding proteins (Tsien, 1980; Nagerl et al., 2000), the concentration of an endogenous Ca^{2+}-binding protein would have to increase such that it provides ≥8 mM of free Ca^{2+}-binding sites, which is unlikely to occur in cortical neurons (Muller et al., 2005).

Together, the speed and the spatial restriction of Ca^{2+} nanodomains helps to activate BKChs fast and transiently and allows for their selective and reliable recruitment by action potentials.

Although BKChs are most probably operated by nanodomains when recruited during action potentials, this does not mean that a BKCh cannot be activated by more than one channel under different conditions. For example, during sustained depolarizations, global (cytoplasmic) Ca^{2+} could rise into the micromolar range (>2 μM) and BKChs would then be activated by Ca^{2+} from several sources pooled in the cytoplasm. Thus, the question arises as to what factors establish the nanodomain operation mode of BKChs? First of all, this obviously requires a special geometry of channels in which one Ca^{2+} channel is situated particularly close to a BKCh such that it dominates the local Ca^{2+} sensed by the BKCh. Second, opening of Ca^{2+} channels by action potentials facilitates nanodomain signaling in two ways. Because of their brief duration, action potentials keep the open time of Ca^{2+} channels short. It has been estimated that N-type Ca^{2+} channels, which couple to hippocampal BKChs (Marrion and Tavalin, 1998), very rapidly close (<0.1ms) as soon as the membrane is repolarized after an action potential (Lee and Elmslie, 1999). This brief open time counteracts the spatial spread of nanodomains. An additional effect of action potentials is that they induce a tail-like single-channel current (Fig. 6). This sharpens nanodomains in time and space and works against an overlap of individual nanodomains. Third, the cooperative action of Ca^{2+} on the open probability of BKChs (Magleby, 2003) facilitates nanodomain operation. This sigmoid dependence makes the BKCh relatively insensitive to small local Ca^{2+} elevation caused by remote channels during that time when the closest channel is shut. In light of the complex interaction of these numerous factors, it can be expected that the tightness of the coupling between BK and Ca^{2+} channels vary among different cell types.

In conclusion, the unique functional role of BKChs in the firing pattern of cortical neurons results from a strategic placement of BKChs in Ca^{2+} nanodomains. This placement is a key to selective Ca^{2+} signaling, rendering BKChs buffer insensitive, and allowing neurons to regulate global Ca^{2+} signals by a high cytoplasmic Ca^{2+}-buffer capacity without affecting the crucial fast repolarization of action potentials.

Appendix

Superposition of multiple microdomains

The aim of this section is to show that the plot of the ln-transformed fractional local Ca^{2+} versus the inverse buffer-length constant will not be a line through the origin when more than one channel contributes to the local Ca^{2+} concentration. Also, it will be illustrated that the following parameters can be graphically estimated from such a plot: the distance of the closest channel, the relative contribution to local Ca^{2+} by the closest channel, and the total number of Ca^{2+} channels contributing to local Ca^{2+}.

We consider a BKCh placed at the origin that is surrounded by $n + 1$ Ca^{2+} channels, which are located at the distances r_j, $j = 0, \ldots, n$. Let r_0 denote the distance of the closest channel such that the following equation is satisfied:

$$0 < r_0 < r_j,\ j = 1, \ldots, n. \tag{16}$$

We assume that the $n + 1$ Ca^{2+} channels are similar with respect to their single-channel conductance and their gating properties and that all channels experience the same membrane potential. We also assume that free Ca^{2+} reaches a near steady-state value fast compared with the mean open time of the channels (see Discussion). In analogy to Equation 1, we can write for the increment in free Ca^{2+} at the origin in the presence of multiple Ca^{2+} channels and in the absence of mobile fibers:

$$\Delta[Ca^{2+}(t)] = \frac{i_{Ca} \times P_o(t)}{4\pi \times F \times D_{Ca}} \left(\frac{1}{r_0} + \sum_{j=1}^{n} \frac{1}{r_j} \right). \tag{17}$$

Because we are interested in the average $[Ca^{2+}]$ over many BKChs, the gating of single channels is summarized in the time-dependent open probability $P_o(t)$ (cf. Neher, 1998). The equation describing the free $[Ca^{2+}]$ in the presence of BAPTA can be obtained by superimposing the contributions of the different Ca^{2+} channels (Neher, 1998), as follows:

$$\Delta[Ca^{2+}(t)]^{BAPTA} = \frac{i_{Ca} \times P_0(t)}{4\pi \times F \times D_{Ca}} \left(\frac{1}{r_0} \exp(-r_0/\lambda) + \sum_{j=1}^{n} \frac{1}{r_j} \exp(-r_j/\lambda) \right). \tag{18}$$

For the fraction of $[Ca^{2+}]$ remaining under BAPTA, we attain the following analogy to Equation 13:

$$\text{norm.}\Delta[Ca^{2+}] := \frac{\Delta[Ca^{2+}(t)]^{BAPTA}}{\Delta[Ca^{2+}(t)]} = \frac{\exp(-r_0/\lambda) \left(1 + r_0 \exp(r_0/\lambda) \sum_{j=1}^{n} \frac{\exp(-r_j/\lambda)}{r_j} \right)}{1 + r_0 \sum_{j=1}^{n} \frac{1}{r_j}}. \tag{19}$$

The logarithmic transformation yields the following:

$$-\ln(\text{norm.}\Delta[Ca^{2+}]) = r_0 \times \frac{1}{\lambda} - \ln \left(\frac{1 + r_0 \sum_{j=1}^{n} \frac{\exp((r_0 - r_j)/\lambda)}{r_j}}{1 + r_0 \sum_{j=1}^{n} \frac{1}{r_j}} \right). \tag{20}$$

If the left side of Equation 20 is plotted versus $1/\lambda$, a graph different from a line results because its initial slope (for $1/\lambda \to 0$) is larger than its asymptotic slope (for $1/\lambda \to \infty$). To determine the initial and the asymptotic slope, we substitute $\nu = 1/\lambda$ ($\lambda > 0$) and

calculate the first derivative of Equation 20 with respect to ν, as follows:

$$\frac{\partial}{\partial \nu}\left[r_0 \times \nu - \ln\left(\frac{1 + r_0 \sum_{j=1}^{n} \frac{\exp(\nu(r_0 - r_j))}{r_j}}{1 + r_0 \sum_{j=1}^{n} \frac{1}{r_j}} \right) \right] = \frac{r_0(1 + \sum_{j=1}^{n} \exp(\nu(r_0 - r_j)))}{1 + r_0 \sum_{j=1}^{n} \frac{\exp(\nu(r_0 - r_j))}{r_j}}. \quad (21)$$

The asymptotic slope of Equation 20 can be obtained by calculating the limit of Equation 21 toward infinity (high BAPTA concentrations), as follows:

$$\lim_{\nu \to \infty} \frac{r_0(1 + \sum_{j=1}^{n} \exp(\nu(r_0 - r_j)))}{1 + r_0 \sum_{j=1}^{n} \frac{\exp(\nu(r_0 - r_j))}{r_j}} = r_0, \quad (22)$$

because, by Equation 16, $(r_0 - r_j) < 0$ for all j.

Thus, the asymptotic slope yields the distance of the closest Ca^{2+} channel, even in the presence of multiple channels. The initial slope of Equation 20 amounts to the following:

$$\lim_{\nu \to 0} \frac{r_0(1 + \sum_{j=1}^{n} \exp(\nu(r_0 - r_j)))}{1 + r_0 \sum_{j=1}^{n} \frac{\exp(\nu(r_0 - r_j))}{r_j}} = r_0 \frac{(1 + n)}{1 + \sum_{j=1}^{n} \frac{r_0}{r_j}} > r_0 \quad (23)$$

by Equation 16, *QED*.

In the presence of high BAPTA concentrations, when λ is sufficiently small (such that $3\lambda < |r_0 - r_j|$, for all j), Equation 20 can be approximated by the following linear equation of the reciprocal buffering length constant:

$$-\ln(\text{norm.}\Delta[Ca^{2+}]) \approx r_0 \times \frac{1}{\lambda} - \ln\left(\frac{1}{1 + \sum_{j=1}^{n} \frac{r_0}{r_j}} \right) = r_0 \times \frac{1}{\lambda} - \ln\left(\frac{\frac{1}{r_0}}{\frac{1}{r_0} + \sum_{j=1}^{n} \frac{1}{r_j}} \right) \quad (24)$$

Compared with Equation 17, it can be seen that the inner logarithmic term in Equation 24 represents the fraction of the local Ca^{2+} at the BKCh contributed by the closest channel located at r_0. Thus, back-extrapolation of the linear portion of the plot of the ln-transformed fractional Ca^{2+} versus $1/\lambda$ to the ordinate supplies the negative logarithm of the relative contribution of the closest channel to the total Ca^{2+} at the origin. Moreover, division of the initial slope (Eq. 23) by the inner logarithmic term (expand by r_0 for clarity) and by the asymptotic slope (Eq. 22) yields an estimate of the total number of Ca^{2+} channels that contribute to the Ca^{2+} increase seen by the BKCh at the origin $(n + 1)$.

It should be noted that this analysis provides reasonable estimates only when most channels are located within ~100 nm around the BKCh. If channels are located beyond that distance, then the condition of near steady-state Ca^{2+} concentrations would be too strongly violated. Furthermore, the correctness of the estimate of the total number of channels requires that the closest channel at r_0 can be well isolated from the others by a buffer concentration that would not result in a too-strong suppression of the Ca^{2+} from the channel at r_0. This is the case when there is a λ^* (i.e., some buffer concentration), with $3\lambda^* < |r_0 - r_j|$, for all j and with $2\lambda^* \geq r_0$.

References

Airaksinen MS, Eilers J, Garaschuk O, Thoenen H, Konnerth A, Meyer M (1997) Ataxia and altered dendritic calcium signaling in mice carrying a targeted null mutation of the calbindin D28k gene. Proc Natl Acad Sci USA 94:1488–1493.

Arnold DB, Heintz N (1997) A calcium responsive element that regulates expression of two calcium binding proteins in Purkinje cells. Proc Natl Acad Sci USA 94:8842–8847.

Augustine GJ, Santamaria F, Tanaka K (2003) Local calcium signaling in neurons. Neuron 40:331–346.

Batini C, Palestini M, Thomasset M, Vigot R (1993) Cytoplasmic calcium buffer, calbindin-D28k, is regulated by excitatory amino acids. NeuroReport 4:927–930.

Beck H, Steffens R, Heinemann U, Elger CE (1997) Properties of voltage-activated Ca2+ currents in acutely isolated human hippocampal granule cells. J Neurophysiol 77:1526–1537.

Carbone E, Lux HD (1987) Kinetics and selectivity of a low-voltage-activated calcium current in chick and rat sensory neurones. J Physiol (Lond) 386:547–570.

Church PJ, Stanley EF (1996) Single L-type calcium channel conductance with physiological levels of calcium in chick ciliary ganglion neurons. J Physiol (Lond) 496:59–68.

Crank J (1975) The mathematics of diffusion. Oxford: Oxford UP.

Dietrich D, Clusmann H, Kral T (2002) Improved hybrid clamp: resolution of tail currents following single action potentials. J Neurosci Methods 116:55–63.

Gollasch M, Hescheler J, Quayle JM, Patlak JB, Nelson MT (1992) Single calcium channel currents of arterial smooth muscle at physiological calcium concentrations. Am J Physiol 263:C948–C952.

Ha TS, Heo MS, Park CS (2004) Functional effects of auxiliary beta4-subunit on rat large-conductance Ca(2+)-activated K(+) channel. Biophys J 86:2871–2882.

Helmchen F, Imoto K, Sakmann B (1996) Ca2+ buffering and action potential-evoked Ca2+ signaling in dendrites of pyramidal neurons. Biophys J 70:1069–1081.

Hille B (1992) Ionic channels of excitable membranes. Sunderland, MA: Sinauer.

Jackson MB, Redman SJ (2003) Calcium dynamics, buffering, and buffer saturation in the boutons of dentate granule-cell axons in the hilus. J Neurosci 23:1612–1621.

Kohr G, Mody I (1991) Endogenous intracellular calcium buffering and the activation/inactivation of HVA calcium currents in rat dentate gyrus granule cells. J Gen Physiol 98:941–967.

Lee HK, Elmslie KS (1999) Gating of single N-type calcium channels recorded from bullfrog sympathetic neurons. J Gen Physiol 113:111–124.

Lesage F, Hibino H, Hudspeth AJ (2004) Association of beta-catenin with the alpha-subunit of neuronal large-conductance Ca2+-activated K+ channels. Proc Natl Acad Sci USA 101:671–675.

Llinas R, Sugimori M, Simon SM (1982) Transmission by presynaptic spike-like depolarization in the squid giant synapse. Proc Natl Acad Sci USA 79:2415–2419.

Lowenstein DH, Miles MF, Hatam F, McCabe T (1991) Up regulation of calbindin-D28K mRNA in the rat hippocampus following focal stimulation of the perforant path. Neuron 6:627–633.

Lu R, Alioua A, Kumar Y, Eghbali M, Stefani E, Toro L (2006) MaxiK channel partners: physiological impact. J Physiol (Lond) 570:65–72.

Maeda H, Ellis-Davies GC, Ito K, Miyashita Y, Kasai H (1999) Supralinear Ca2+ signaling by cooperative and mobile Ca2+ buffering in Purkinje neurons. Neuron 24:989–1002.

Magleby KL (2003) Gating mechanism of BK (Slo1) channels: so near, yet so far. J Gen Physiol 121:81–96.

Marrion NV, Tavalin SJ (1998) Selective activation of Ca2+-activated K+ channels by co-localized Ca2+ channels in hippocampal neurons. Nature 395:900–905.

Matveev V, Zucker RS, Sherman A (2004) Facilitation through buffer saturation: constraints on endogenous buffering properties. Biophys J 86:2691–2709.

Muller A, Kukley M, Stausberg P, Beck H, Muller W, Dietrich D (2005) Endogenous Ca^{2+} buffer concentration and Ca^{2+} microdomains in hippocampal neurons. J Neurosci 25:558–565.

Nagerl UV, Novo D, Mody I, Vergara JL (2000) Binding kinetics of calbindin-D(28k) determined by flash photolysis of caged Ca(2+). Biophys J 79:3009–3018.

Naraghi M (1997) T-jump study of calcium binding kinetics of calcium chelators. Cell Calcium 22:255–268.

Naraghi M, Neher E (1997) Linearized buffered Ca^{2+} diffusion in microdomains and its implications for calculation of $[Ca^{2+}]$ at the mouth of a calcium channel. J Neurosci 17:6961–6973.

Neher E (1986) Concentration profiles of intracellular calcium in the presence of a diffusible chelator. In: Calcium electrogenesis and neuronal functioning (Heinemann U, Klee M, Neher E, Singer W, eds), pp 80–96. Berlin, Heidelberg: Springer.

Neher E (1995) The use of fura-2 for estimating Ca buffers and Ca fluxes. Neuropharmacology 34:1423–1442.

Neher E (1998) Usefulness and limitations of linear approximations to the understanding of Ca++ signals. Cell Calcium 24:345–357.

Nowycky MC, Pinter MJ (1993) Time courses of calcium and calcium-bound buffers following calcium influx in a model cell. Biophys J 64:77–91.

Pape PC, Jong DS, Chandler WK (1998) Effects of partial sarcoplasmic reticulum calcium depletion on calcium release in frog cut muscle fibers equilibrated with 20 mM EGTA. J Gen Physiol 112:263–295.

Partridge LD, Muller TH, Swandulla D (1994) Calcium-activated non-selective channels in the nervous system. Brain Res Brain Res Rev 19:319–325.

Patton C, Thompson S, Epel D (2004) Some precautions in using chelators to buffer metals in biological solutions. Cell Calcium 35:427–431.

Prakriya M, Lingle CJ (2000) Activation of BKChs in rat chromaffin cells requires summation of Ca(2+) influx from multiple Ca(2+) channels. J Neurophysiol 84:1123–1135.

Protti DA, Uchitel OD (1997) P/Q-type calcium channels activate neighboring calcium-dependent potassium channels in mouse motor nerve terminals. Pflügers Arch 434:406–412.

Roberts WM (1993) Spatial calcium buffering in saccular hair cells. Nature 363:74–76.

Roberts WM (1994) Localization of calcium signals by a mobile calcium buffer in frog saccular hair cells. J Neurosci 14:3246–3262.

Robitaille R, Garcia ML, Kaczorowski GJ, Charlton MP (1993) Functional colocalization of calcium and calcium-gated potassium channels in control of transmitter release. Neuron 11:645–655.

Sah P (1996) Ca(2+)-activated K+ currents in neurones: types, physiological roles and modulation. Trends Neurosci 19:150–154.

Sah P, Faber ES (2002) Channels underlying neuronal calcium-activated potassium currents. Prog Neurobiol 66:345–353.

Shao LR, Halvorsrud R, Borg-Graham L, Storm JF (1999) The role of BK-type Ca2+-dependent K+ channels in spike broadening during repetitive firing in rat hippocampal pyramidal cells. J Physiol (Lond) 521:135–146.

Simon SM, Llinas RR (1985) Compartmentalization of the submembrane calcium activity during calcium influx and its significance in transmitter release. Biophys J 48:485–498.

Stern MD (1992) Buffering of calcium in the vicinity of a channel pore. Cell Calcium 13:183–192.

Storm JF (1987a) Action potential repolarization and a fast after-hyperpolarization in rat hippocampal pyramidal cells. J Physiol (Lond) 385:733–759.

Storm JF (1987b) Intracellular injection of a Ca2+ chelator inhibits spike repolarization in hippocampal neurons. Brain Res 435:387–392.

Tsien RY (1980) New calcium indicators and buffers with high selectivity against magnesium and protons: design, synthesis, and properties of prototype structures. Biochemistry 19:2396–2404.

Vergara C, Latorre R, Marrion NV, Adelman JP (1998) Calcium-activated potassium channels. Curr Opin Neurobiol 8:321–329.

Xia XM, Fakler B, Rivard A, Wayman G, Johnson-Pais T, Keen JE, Ishii T, Hirschberg B, Bond CT, Lutsenko S, Maylie J, Adelman JP (1998) Mechanism of calcium gating in small-conductance calcium-activated potassium channels. Nature 395:503–507.